Statistical fault detection in photovoltaic systems

Elyes Garoudja [a], Fouzi Harrou [b], Ying Sun [b], Kamel Kara [a], Aissa Chouder [c], Santiago Silvestre [d]

[a] SET Laboratory, Electronics Department, Blida 1 University, BP 270 Blida, Algeria

[b] King Abdullah University of Science and Technology (KAUST), Computer, Electrical and Mathematical Sciences and Engineering (CEMSE) Division, Thuwal 23955-6900, Saudi Arabia

[c] Electrical Engineering Laboratory (LGE), University Mohamed Boudiaf of M'sila, BP 166, 28000, Algeria

[d] Electronic Engineering Department, Universitat Politècnica de Catalunya, C/ Jordi Girona 1-3, Campus Nord UPC, 08034 Barcelona, Spain

Keywords: Fault detection;Temporary shading;Photovoltaic systems;One-diode model

Statistical monitoring charts

A b s t r a c t

Faults in photovoltaic (PV) systems, which can result in energy loss, system shutdown or even serious safety breaches, are often difficult to avoid. Fault detection in such systems is imperative to improve their reliability, productivity, safety and efficiency. Here, an innovative model-based fault-detection approach for early detection of shading of PV modules and faults on the direct current (DC) side of PV systems is proposed. This approach combines the flexibility, and simplicity of a one-diode model with the extended capacity of an exponentially weighted moving average (EWMA) control chart to detect incipient changes in a PV system. The one-diode model, which is easily calibrated due to its limited calibration parameters, is used to predict the healthy PV array's maximum power coordinates of current, voltage and power using measured temperatures and irradiances. Residuals, which capture the difference between the measurements and the predictions of the one-diode model, are generated and used as fault indicators. Then, the EWMA monitoring chart is applied on the uncorrelated residuals obtained from the one-diode model to detect and identify the type of fault. Actual data from the grid-connected PV system installed at the Renewable Energy Development Center, Algeria, are used to assess the performance of the proposed approach. Results show that the proposed approach successfully monitors the DC side of PV systems and detects temporary shading.

1. Introduction

1.1. The state of the art

Traditional sources of energy, such as oil, coal and nuclear energy, have negative effects on human health, biodiversity, ecosystems and climate change. Nonetheless, industrial growth has extensively increased global consumption of fossil fuels, and the concomitant impacts on human health and the environment (Johansson, 1993). Renewable energy sources such as solar, wind and

biomass, are promising alternatives to conventional fossil fuels because they are clean, sustainable, safe, and environment-friendly with zero CO2 emissions (Panwar et al., 2011). One of the most sustainable and economically competitive renewable energy sources is solar photovoltaic (PV) energy (Zhao et al., 2015). Moreover, solar PV energy increases a country's energy security by reducing dependence on fossil fuels.

Under practical conditions, faults are unavoidable in PV systems, particularly on the direct current (DC) side where open circuit faults, short circuits faults, hotspot faults, and total and partial shading faults are possible (Chouder and Silvestre, 2010; Hachana et al., 2016; Silvestre et al., 2015; Yahyaoui and Segatto, 2017). Faults on the DC side of PV systems can result in energy loss, system shutdown and even in serious safety breaches (Brooks, 2011; Alam et al., 2015). For example, two PV facilities in the US (a 383 KWp PV array in Bakersfield, CA and a 1.208 MWp power plant in Mount Holly, NC) burned in 2009 and 2011, respectively (Brooks, 2011). The source for these accidents was a fault on the DC side that was not identified early (Vergura et al., 2009; Hariharan et al., 2016). If such faults in PV systems are not detected promptly, they can affect the system's efficiency and profitability, as well as the health and safety of workers and community members.

The detection of faults in PV systems is therefore crucial for maintaining normal operations by providing early fault warnings. Indeed, accurate and early detection of faults in a PV system is critical to avoid the progression of faults and to reduce considerably productivity losses.

Several fault detection techniques for PV systems have been developed. They are two main types of these techniques: process history-based approaches and model-based approaches. Processhistory- based methods use implicit empirical models derived from analysis of available data and rely on computational intelligence

and machine learning methods (Mekki et al., 2016; Shrikhande et al., 2016; Hare et al., 2016; Suganthi et al., 2015; Silvestre et al., 2014; Tadj et al., 2014; Zhao et al., 2013). Mekki et al. (2016) proposed an artificial neural network to evaluate PV system performance under partial shading conditions. Chine et al. (2016) used an artificial neural network to detect short circuits in PV arrays. Tadj et al. (2014) proposed a fault-detection approach based on fuzzy logic to detect possible solar panel abnormalities.

Pavan et al. (2013) used a Bayesian neural network and polynomial regression to predict the effect of soiling in large-scale PV system. However, process-history-based methods require the availability of a relevant dataset that describes both healthy and faulty operating conditions in a PV system.

On the other hand, model-based approaches compare analytically computed outputs with measured values and signal an alarm when large differences are detected (Harrou et al., 2014). Several model-based approaches to fault detection in PV systems have been reported in the literature using the one-diode model (Chouder and Silvestre, 2010; Vergura et al., 2009; Chouder and Silvestre, 2009; Chao et al., 2008). In one-diode-based fault detection approaches, model

parameters are determined by parameter extraction methods from weather conditions and the datasheet from the PV module manufacturer (Garoudja et al., 2015; Abou et al., 2015; Chouder and Silvestre, 2010). Both irradiance and solar panel temperature measurements are needed for such approaches to predict the maximum power point (MPP) of the PV system. Kang et al. (2012) used a Kalman filter to predict the power output of a PV system. Johnson et al. (2011) used a Fourier series to detect arc faults in a PV system. Other approaches employed sophisticated tools, such as time-domain reflectometry (TDR) (Munoz et al.,2011) and thermoreflectance imaging (TR) (Hu et al., 2014). The TR method was proposed to detect the appearance of hot spots inside PV systems (Hu et al., 2014). The TDR approach can detect,localize, and diagnose faults in PV systems, but the system must be turned off, which affects system productivity. TDR also requires sophisticated tools to introduce the input signal. Of course, the effectiveness of model-based fault-detection approaches relies on the accuracy of the models used.

1.2. Motivation and contributions

Until recently, statistical process control charts have not been widely used to monitor the performance of PV systems. Zhao et al. (2013) proposed a statistical technique using three outlier rules to classify deviations. Recently, Platon et al. (2015) proposed to use the three-sigma rule for online fault detection in PV systems.

However, the three-sigma rule, also known as the Shewhart chart (Montgomery, 2007), loses the ability to detect incipient faults in process data because it makes decisions based only on information about the process in the last observation. Incorporating information about the entire process history, including previous or recent observations, into the decision rule can help to improve sensitivity to small shifts. The exponentially weighted moving average

(EWMA) scheme incorporates information from the entire process history, rather than using only the most recent observation. This makes it more sensitive than the Shewhart chart to small anomalies. The main contribution of this work is to exploit the advantages of the exponentially weighted moving average (EWMA) chart and those of one-diode modeling for enhancing detection performances of PV systems, especially for detecting small faults in DC side of PV system and shading fault. Such a choice is mainly motivated by the greater ability of the EWMA metric to detect small fault in process mean, which makes it very attractive as fault detection approach. Note that the main advantage of EWMA chart is that it can be easily implemented in real time because of the low computational cost, which is not the case in a classifiers based methods (the classifier algorithms are performed offline rather than online). A decision can be made for each new sample by comparing the value of the EWMA decision statistic with the value of the threshold.

An anomaly is declared if the EWMA statistic exceeds the threshold. To do so, residuals, which are the differences between the measured and predicted MPP for the current, voltage and power, from the PV array simulation model are generated. Under normal operating conditions, the residuals in a PV system are close to zero due to measurement noise and errors, while they significantly deviate from zero when the system is faulty. Residuals are used as fault indicators.

Then, an EWMA chart is used to monitor the residuals to reveal abnormalities. Once the fault has been detected, the next step is expected to determine its cause. The proposed approach can also effectively diagnose fault types based on the output DC current and voltage. Indeed, fault diagnosis can help the operators and engineers in the process-monitoring scheme and therefore significantly reduce the risk of safety problems or loss in profitability. The proposed fault detection strategy has been validated using measurements from the 9.54 kWp PV plant at the Renewable Energy Development Center in Algiers, Algeria. The remainder of this paper is organized as follows. Section 2 gives a brief overview of the grid-connected PV plant that provided data for this study. In Section 3, one-diode model is reviewed. Section 4 introduces the EWMA chart and its use in fault detection. Section 5 applies the proposed fault-detection and diagnosis procedure to the PV plant in Algeria. Finally, Section 6 concludes with a discussion and suggestions for future research directions.

2. The grid-connected PV system in Algiers, Algeria

We assessed our fault detection method using practical data collected from a grid-connected photovoltaic (GCPV) system located at Renewable Energy Development Center (CDER) in Algiers, Algeria. This PV system operates from June 21st, 2004, and the output power by this system is injected directly into the national electric distribution network without any storage device.

This 90 module PV system 106 Wp is installed on the roof of the CDER building as shown in Fig. 1. This 9.54 kWp rated system has an output DC voltage of 125–450 V and an output AC voltage of 220 V. It comprises three sub-arrays of 30 modules each. The outputs of these three sub-arrays are connected to a single-phase 2.5 KW PV inverter (IG30 Fronius). Each sub-array consists of 30 Isofoton (106 W-12 V) PV modules, which are grouped into two parallel strings of fifteen PV modules in series. Irradiance measurements are collected with a Kipp & Zonen CM11 thermoelectric pyranometer and the temperature is measured with a K-type thermocouple.

An Agilent 34970A data logger acquires the data through a connection to the local grid through an inverter, a safety control box and a meter. When the utility grid is not energized the inverter immediately stops providing power to the grid. The main components of the GCPV system are shown in Fig. 2. The data from only one sub-array are used to simulate both healthy and faulty operating conditions under various meteorological conditions. The electrical characteristics of the Isofoton 106–12 PV module are summarized in Table 1.

The standard test conditions for these solar panels were determined at 25 ºC and solar irradiance of 1000 W/m2. The real measurements (ie., MPP voltage and current) were collected every second.

Table 1
Electrical characteristics of the Isofoton 106-12 PV module under standard test condition.

Electrical characteristics of the solar panels tested in this study	Value
Peak power (PMPP)	106W
Voltage at maximum power point (VMPP)	17.4 V
Current at maximum power point (IMPP)	6.10 A

Open circuit voltage (Voc)	21.6 V
Short circuit current (Isc)	6.54 A

Fig. 1. The PV array installed on the roof of the CDER building in Algiers, Algeria (Arab et al., 2005).

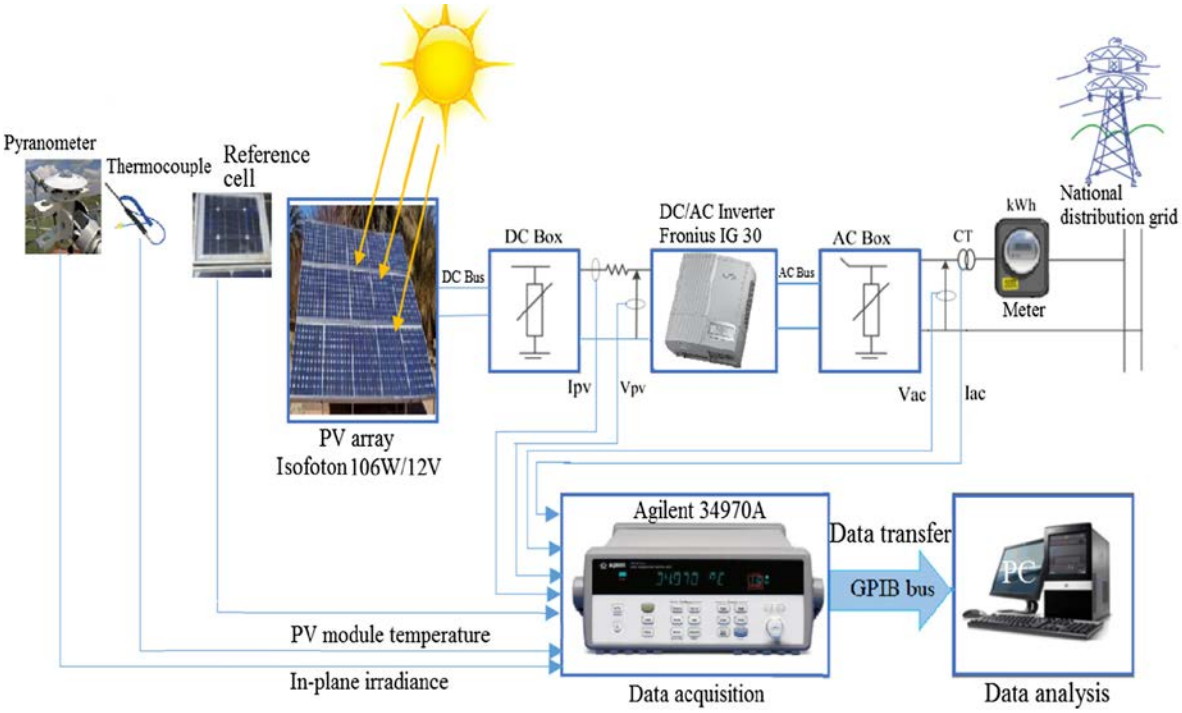

Fig. 2. The main components of grid-connected PV system used in this study.

2.1. Typical faults in PV systems

Generally, a PV system can be affected by different types of faults that can result in significant loss of power in a PV system.

According to the fault duration, two types of faults can be distinguished: temporary and permanent faults. Temporary faults, such as shading, disappear after a certain period of time or after being manually cleared in cases of dust, leaves or bird dropping. The PV system then returns to its normal operating conditions. On the other hand, permanent faults, including short circuits and open circuits are persistent or ongoing. Three well-known faults commonly occurred in the DC side of PV systems (short circuits, open circuits and partial shading) are studied in this paper (see Fig. 3).

A short-circuit fault can affect cells, bypass diodes or modules. It is mainly due to the infiltration of water into modules or to bad wiring between the module and the inverter. Additionally, aging of PV modules, which is caused by long-term operation of the PV system, is one of the main sources of short-circuit faults. For example, there is a short-circuit fault at point 'F1' on the second string on thright of the PV array in Fig. 3.

An open-circuit fault may occur if any current path that is in series to the load is accidentally removed or opened from a closed circuit. Such a situation mainly occurs due to a break in wires between PV modules or solar cells. An example of an open circuit fault is shown at point at 'F2' in Fig. 3. Open-circuit faults occur when a conductor is accidentally removed from the closed circuit.

A partial shading fault occurs when part of the PV array is shaded while the other part is normally exposed to the solar irradiance. This occurs due to several reasons including passage of clouds, dirt on PV modules, snow, or any other light barrier. Nearby obstacles might also interfere and cast shadows, resulting in reduced power output. Even a small amount of shade can dramatically reduce the output amperage of a PV system.

3. PV module modeling

Numerous models have been reported in the literature that model energy production of PV cells. The one-diode model (ODM) is the most common model used to predict energy production from PV cells (Duffie and Beckman, 2013). This model is based on modeling the solar cell as a light-generated current source connected in parallel with a diode with series and parallel resistances accounting for resistive losses (see Fig. 4).

ODM determines the resulting current and voltage given the parameters of the solar cell (McEvoy et al., 2012) as follows:

$$I = I_{ph} - \underbrace{I_0\left[\exp\left(\frac{q(V+R_sI)}{nk_BT}\right)-1\right]}_{I_d} - \underbrace{\frac{V+R_sI}{R_{sh}}}_{I_{sh}}, \qquad (1)$$

where I and V are the generated current and voltage of the solar cell, respectively. Iph, also called the photogenerated current, corresponds to the amount of current generated by incoming photons; it is proportional to the irradiance and the area of the solar cell. I0 is the dark saturation current, n is the diode's ideality factor. Rs and Rsh are the series and shunt resistances, respectively. kB is Boltzmann's constant (kB = 1:38064852 10^{-23} J K^{-1}). T is the cell's temperature and q is the electronic charge (q = 1:60217662 10^{-19} C).

The simulation of a PV array is comprised of three stages summarized next.

Step 1 : Model parameters extraction

ODM in Eq. (1) depends on the values of five unknown

parameters (Iph; I0; n, Rs and Rsh), which determine the overall performance of a solar cell. These parameters are not provided in the manufacturer's datasheet. Hence, accurate extraction of these parameters is a crucial step in PV system modeling. Indeed, solar cell parameters extraction could be defined as an optimization problem, wherein the cost function to be minimized is defined as the root mean square error (RMSE) between the measured and the predicted I-V curves by ODM.

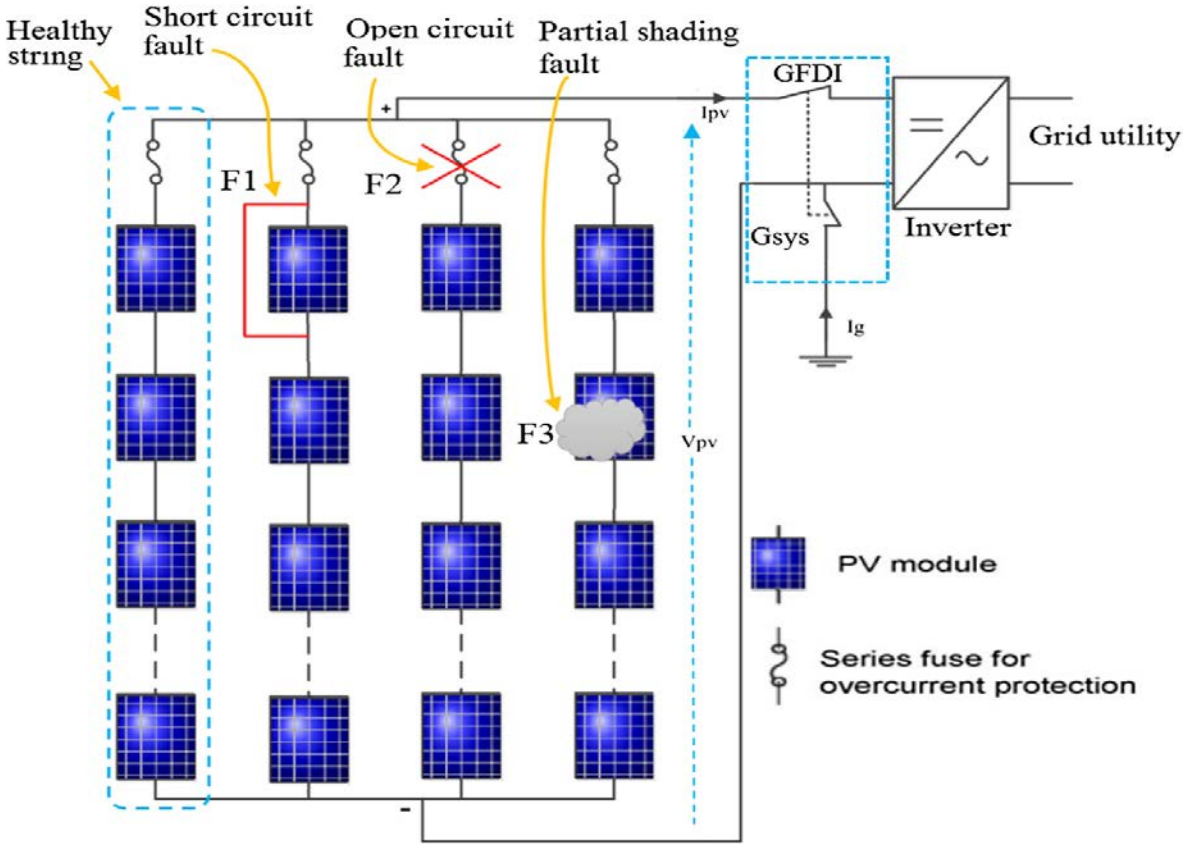

Fig. 3. The faulty operating cases considered in this paper.

$$RMSE = \sqrt{\frac{1}{m}\sum_{i=1}^{m}[f_i(I_{meas}, V_{meas}, \theta)]^2}, \tag{2}$$

where

$$f(I_{meas}, V_{meas}, \theta) = I_{meas} - \left\{ I_{ph} - I_0 \left[\exp\left(\frac{q(V_{meas} + R_s I_{meas})}{n k_B T} \right) - 1 \right] - \frac{V_{meas} + R_s I_{meas}}{R_{sh}} \right\}, \tag{3}$$

Imeas and Vmeas are the measured output current and voltage of the reference PV module respectively (they define the static

I-V curve measurements of the reference PV module), h is the vector of the five unknowns electrical parameters [Iph; I0; n, Rs and Rsh], m stands for the number of experimental data used in the parameters extraction process. The static I-V curve of a reference PV module are measured using an I-V curve tracer when the module is isolated from the inverter.
In practice, I-V curve tracer takes less than one second to measure the current–voltage (I-V) characteristic of the tested PV module. Of course, the aim of this optimization is to find the optimal parameters values that minimize the objective function and provides the lowest RMSE value. In this paper,these five parameters have been extracted using the Artificial Bee Colony (ABC) algorithm (Garoudja et al., 2015; Abouet al., 2015) on the basis of the real measured static (I-V) data, the predicted data obtained from the one diode model and the available parameters in Table 1.

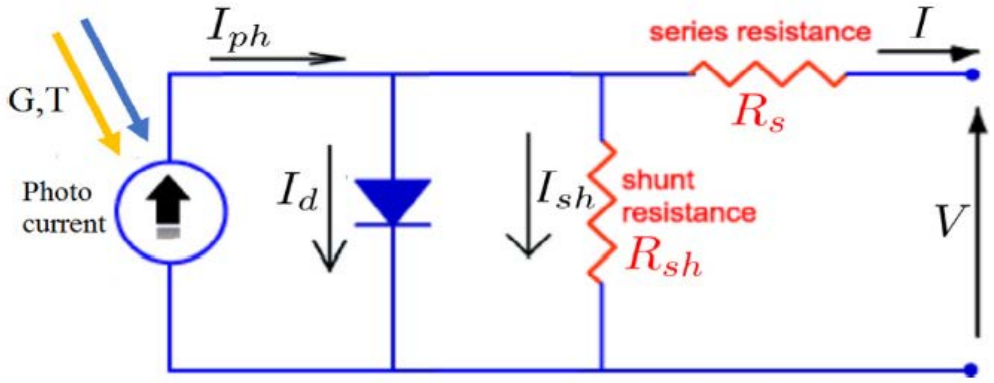

Fig. 4. Equivalent circuit of a solar cell based on a current source and a diode, with losses represented by series and parallel resistance.

Step 2 : Model simulation.
The identified parameters via ABC algorithm, which are given in Table 2, are used to predict the MPP coordinates of current, voltage and power of the entire PV array. The PV array model is simulated using PSIMTM/MatlabTM cosimulation. Using this co-simulation, the entire PV array is physically constructed (physical PV modules) as two parallel PV string, of fifteen PV modules each. This model relies on access to both irradiance and solar panel temperature measurements to predict the MPP coordinates.
Step 3 : Model validation
Model validation is possibly the most important step in PV array modeling. In this step, the ability of the simulated model to mimic accurately the real behavior of the monitored PV plan is evaluated. Specifically, the identified ODM parameters are used to build the entire PV array cosimulation model, then this later is used to mimic the real PV array behavior under different meteorological conditions.
The input variables of the simulated model consist of real measured meteorological conditions of temperatures and irradiances. The output variables are the PV array MPP coordinates of current, voltage and power. The predicted MPP coordinates of voltage and power obtained from the simulated model are then compared to the real measured MPP coordinates collected from the real PV array. Here, the co-simulation model is fitted to the fault-free data from the GCPV system described above. Fig. 5(a) and (b) respectively shows the measured and predicted DC current and DC power for a cloudy day, June 24, 2008. This figure shows that the model suitably fits the measured data, thus indicating that the selected parameters are satisfactory. This figure also shows that after sunset and during periods of negligible irradiances, the system

completely shuts down. This is done to reduce power consumption and thereby increase overall efficiency. Scatter plot of the measured and predicted DC current and DC power are presented in Fig. 6(a) and (b). These plots indicate that the PV array simulation model predicts the measured DC current and DC power well.

Table 2
Extracted PV module parameters.

PV parameters	I_{ph} [A]	I_0 [A]	n	R_s [Ω]	R_{sh} [Ω]
Value	6.54	1.11e−05	1.66	0.1474	202.6

In addition, to evaluate the quality of the simulation model with the selected parameters, three numerical criteria are used: R2, the mean absolute percent error (MAPE) and RMSE. These were calculated as follows:

$$R^2 = 1 - \frac{\sum_{t=1}^{m}(y_t - \hat{y}_t)^2}{\sum_{t=1}^{m}(y_t - mean(Y))^2}, \quad (4)$$

$$RMSE = \sqrt{\frac{\sum_{t=1}^{m}(y_t - \hat{y}_t)^2}{m}}, \quad (5)$$

$$MAPE = 100\left[\sum_{t=1}^{m}\left(\frac{|y_i - \hat{y}_i|}{|y_i|}\right)\right] \Big/ m, \quad (6)$$

where yt are the measured values, ^yt are the corresponding predicted values by the simulation model and m is the number of samples.
Goodness-of-fit results for the three cells studied are presented in Table 3.
Results in Table 3 show that the PV array simulation model with the selected parameters captures the measured DC current and power. The r2 values above 0.9, the low RMSE of 0.1932 and the low MAPE of 6.57% demonstrate that ODM provides good predictive quality.

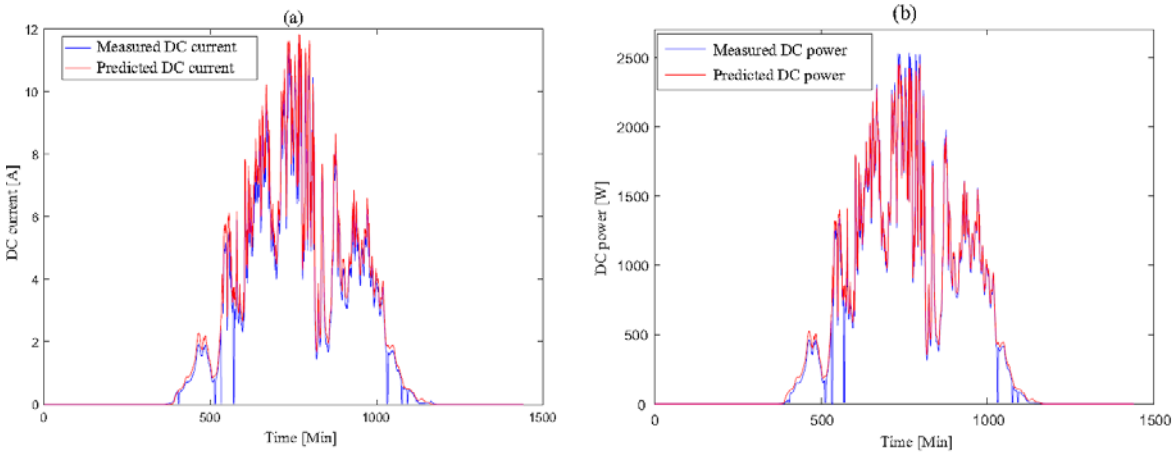

Fig. 5. Measured and predicted plot of DC current (a) and DC power (b) for June 24, 2008.

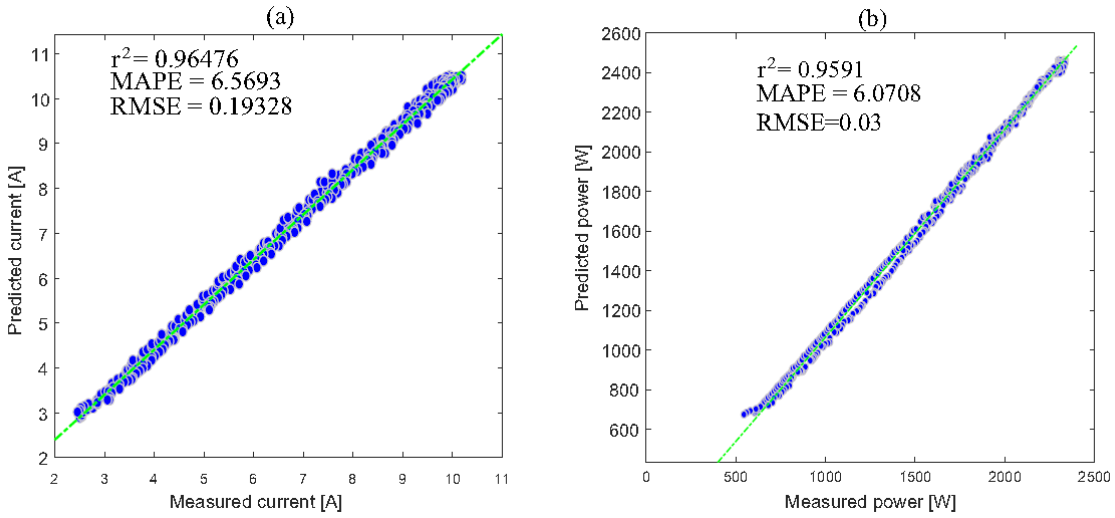

Fig. 6. Scatter plot of the measured and predicted DC current (a) and DC power (b) for June 24, 2008.

Table 3
Statistical validation metrics applied to data in Fig. 6.

	DC current	Power current
r^2	0.96	0.96
RMSE	0.193	0.03
MAPE	6.57	6.07

4. Fault detection approaches

The overarching goal of this paper is to improve the PV system efficiency by monitoring its DC side in an efficient manner. Traditionally in manufacturing industries, statistical quality control is used for monitoring and controlling product quality. Furthermore, statistical process control charts can provide early warnings of abnormal changes in system operations, helping operators to identify the onset of potential faults, such as short circuits, open circuits, sensor bias and shading faults. These statistical charts include Shewhart, cumulative sum (CUSUM), and EWMA charts. Univariate statistical methods, such as the Shewhart chart and EWMA, have been widely used to monitor industrial processes for many years (Montgomery, 2005). These methods are briefly introduced here.

4.1. Shewhart monitoring chart

In a Shewhart chart, a sequence of samples (denoted as xi) is plotted against time (Montgomery, 2005). Upper and lower control limits for the samples are established around the process mean (l) based on the three-sigma rule, i.e., UCL /LCL = $\mu 0 \pm \sigma 0$, where σO is the standard deviation of the fault-free data computed when the process is running under healthy conditions. Whenever the most recent measured point or a consecutive sequence of points is outside the control limits, an

abnormal condition is encountered and attention is focused on diagnosing the source of the problem.

Here, the Shewhart chart is used as a benchmark for fault detection in the DC side of a PV system. In the next section, EWMA chart and its use in fault detection will be briefly described.

4.1.1. EWMA monitoring chart

In this section, the basic idea of the EWMA chart and its properties are introduced. For a more detailed discussion about its design, implementation and properties, refer to (Montgomery, 2005; Reynolds and Stoumbos, 2005; Lucas and Saccucci, 1990; Hunter, 1986). EWMA is constructed based on exponential weighting of available observations, a design that provides improved sensitivity to small changes in the mean of a multivariate process.

EWMA charts are able to detect small shifts in the process mean because the EWMA statistic is a time-weighted average of all previous observations. The EWMA control scheme was first introduced by Roberts (Hunter, 1986; Lucas and Saccucci, 1990), it has been extensively used in time series analysis. The EWMA monitoring monitoring chart is an anomaly-detection technique widely used by scientists and engineers in various disciplines (Kadri et al., 2016; Zerrouki et al., 2016; Harrou et al., 2015; Harrou and Nounou, 2014; Montgomery, 2005). Assume that fx1; x2; . . . ; xng are individual observations collected from a monitored process. The expression for EWMA is (Montgomery, 2005):

$$\begin{cases} z_t = & \lambda x_t + (1-\lambda)\, z_{t-1} & \text{if } t > 0 \\ z_0 = & \mu_0, & \text{if } t = 0. \end{cases} \tag{7}$$

The starting value, z0, is usually set to be the mean of fault-free data, l0. zt is the output of EWMA and xt is the observation from the monitored process at the current time. The forgetting parameter $\lambda \in [0; 1]$ determines how fast EWMA forgets the data history.

From Eq. (7), it is easy to see that

$$\begin{aligned} z_t &= \lambda x_t + (1-\lambda)\overbrace{[\lambda x_{t-1} + (1-\lambda) z_{t-2}]}^{z_{t-1}} \\ &= \lambda x_t + \lambda(1-\lambda) x_{t-1} + (1-\lambda)^2 z_{t-2}. \end{aligned}$$

Using Eq. (7) recursively, we find that the EWMA is a linear combination of the observations:

$$\begin{aligned} z_n = {} & \lambda x_n + \lambda(1-\lambda) x_{n-1} + \lambda(1-\lambda)^2 x_{n-2} + \cdots + \lambda(1-\lambda)^{n-1} x_1 \\ & + (1-\lambda)^n \mu_0 \end{aligned} \tag{8}$$

Eq. (8) can also be written as:

$$z_t = \lambda \sum_{t=1}^{n} (1-\lambda)^{n-t} x_t + (1-\lambda)^n \mu_0, \tag{9}$$

where $\lambda\,(1-\lambda)^{1-t}$ is the weight for xt , which decreases off exponentially for past observations. In other words, as time passes the smoothed statistic zt becomes the weighted average of a greater and greater number of the past observations x_{t-n}, and the weights assigned to previous observations are in general proportional to the terms of the geometric progression

$$\left\{\lambda, \lambda(1-\lambda), \lambda(1-\lambda)^2, \lambda(1-\lambda)^3, \ldots\right\}$$

A geometric progression is the discrete version of an exponential function, so this is where the name for this method originated. The weighting for older data point decrease exponentially, giving much more important to recent observation while still not discarding older observation entirely. It can be seen that if k is small, more weight is assigned to past observations and the chart is efficient at detecting small changes in the process mean. On the other hand, if k is large, more weight is assigned to the current observation and less weight is assigned to its previous observations. The chart is thus able to detect large shifts (Montgomery, 2005; Kadri et al., 2016). In the special case when k ¼ 1, EWMA is equal to the most recent observation, xt , and provides the same results as the Shewhart chart provides. As k approaches zero, EWMA approximates the CUSUM criteria, which give equal weight to historical observations.
Under fault-free conditions, the standard deviation of zt is defined as

$$\sigma_{z_t} = \sigma_0 \sqrt{\frac{\lambda}{(2-\lambda)}[1-(1-\lambda)^{2t}]}, \qquad (10)$$

However, in the presence of a mean shift at the time point,

$$z_t \sim \mathcal{N}\left(\mu_0 + \left[1-(1-\lambda)^{n-\tau+1}\right](\mu_1-\mu_0), \sigma_{z_t}^2\right). \qquad (11)$$

It can be seen from Eq. (11) that the mean of the EWMA statistic in the presence of faults is a weighted average of l0 and l1, and the weight of l1 is larger when n is larger. Therefore, the EWMA statistic, zt , indeed contains useful information about the mean shift.

The upper and lower control limits of the EWMA chart for detecting a mean shift are

$$UCL/LCL = \mu_0 \pm L\sigma_{z_t},$$

4.2. ODM-based EWMA for PV monitoring

In general, the model is first built and then fault diagnosis procedures is performed accordingly. The estimation of the residuals, which is crucial in model-based fault detection, depends on the appropriate system modeling. Once ODM is built based on data representing historically normal operations and validated, it can be used to monitor future deviations in the system. Here, the advantages of ODM with those of the EWMA monitoring chart are combined, which should result in an improved fault detection system, especially for detecting small changes. Specifically, in this approach, the EWMA chart is employed for fault detection to indicate how well the measurements conform to the model or how large the deviation from the normal model is. Towards this end, the EWMA chart is applied to monitor residuals obtained from ODM (see Fig. 7).
The differences between the real measured and predicted MPP current, MPP voltage and MPP power obtained from the simulated model are the residuals that can be used as indicators to detect a possible fault.

$$\widetilde{I}_t = I_t - \widehat{I}_t, \quad \widetilde{V}_t = V_t - \widehat{V}_t, \quad \widetilde{P}_t = P_t - \widehat{P}_t, \quad t \in [1, n], \qquad (13)$$

where It and bI t are the measured and predicted MPP current, respectively, and Vt and bVt are the measured and predicted MPP voltage; and Pt and bPt are the measured and predicted peak power.

In this work, the residuals are used as fault indicators. Indeed, under normal operation, the residuals are close to zero due to measurement noise and errors, while they significantly deviate from zero in the presence of abnormal events. The implementation of the developed monitoring methods comprises two stages: off-line modeling and on-line monitoring. In the off-line modeling phase, ODM is used on the normal operating data (training data), enabling us to obtain a reference model. Then, the fault detection procedure is executed by using the reference simulated model with the EWMA chart in the on-line monitoring phase. The ODM-EWMA fault detection algorithm is summarized in Table 4.

To improve system operations, we want not only to monitor the system in an efficient manner but also to identify the type of fault that results in any degradation of the PV system, including declines in operation reliability, and profitability, such that we can respond accordingly by making any necessary correction to the system.

Towards this end, the EWMA chart is applied based on the residual of output DC power to detect the presence of faults. Then, the type of fault is identified by analyzing the monitoring results of the EWMA chart when it is applied to the residuals of output DC current and voltage. The fault identification procedure is summarized in Fig. 8.

The proposed strategy tests at the first stage the peak power to detect a fault. This choice is mainly due to the fact that faults affect inevitably the peak power. Thus, the peak power is used as a fault indicator in the detection phase. On the other hand, both DC output current and voltage are unsuitable to be used as sensitive indicators in this phase. For example, when a short circuit occurs in one PV module from a string, current indicator value will not be significantly changed from its healthy set point. Meanwhile, a substantial change will appear in the power indicator (peak of power).

Besides, the same situation occurs when a string is completely disconnected. Indeed, the DC output voltage remains unaltered regarding its healthy status in contrast to the peak power decrease significantly. Moreover, the ranking of the current and voltage indicators is unimportant in the fault diagnosis phase.

5. Results and discussion

5.1. Detection results

The proposed fault detection scheme is validated using practical data collected from the 9.54 kWp GCPV system installed at CDER in Algeria (see Section 2). In this section, the ability of the EWMA chart to detect the presence of faults in the data and to identify the type of detected fault is assessed. To assess the strength of the EWMA-based monitoring chart, three case studies involving different types of faults were conducted. In the first case study, it is assumed that the PV system contains one or more short-circuited PV module (case A). In the second case study, an open-circuit PV string is considered (case B). In the third case study, the monitored PV system is exposed to temporary shadowing (case C).

Table 4
EWMA-based fault detection algorithm for PV system monitoring.

(1) **Given**
- Real measurement of irradiance and module temperature
- Real measurement of maximum power point (MPP) values of current, voltage and power collected from the PV plant under normal operating conditions
- Module parameters obtained from the PV module datasheet (see Table 1)

(2) **Build ODM using the fault-free training data**
- Extract electrical parameters for the five-parameter model based on the measured cell temperature and irradiance collected from the monitored PV system under normal operating conditions (see Section 2) using the Artificial Bee Colony (ABC) algorithm (Garoudja et al., 2015). The extracted parameters are then used to simulate the PV system
- Compute the residuals between the measured and the predicted DC current, DC voltage and DC power (I_{mpp}, V_{mpp} and P_{mpp}) from the constructed model using fault-free data
- Compute the control limits for the EWMA chart using Eq. (12)

(3) **Test the new data**
- Generate residual vectors, $\bar{I}, \bar{V}$ and $\bar{P}$, using the selected five-parameter-based model
- Compute the EWMA monitoring statistic for the new data using Eq. (7)

(4) **Check for faults**
- Declare a fault when the EWMA decision statistic for the new data exceeds the control limits

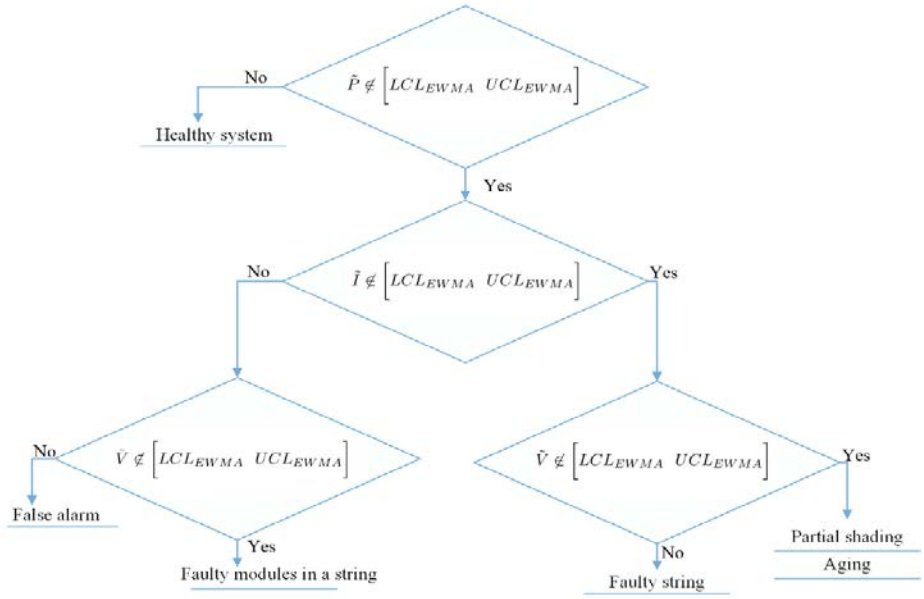

Fig. 8. Fault identification procedure.

5.1.1. Normal operating conditions

Monitoring results from ODM-based Shewhart chart under normal operating conditions are shown in Fig. 9(a)–(c), monitoring results from the EWMA chart under normal operating conditions are presented in Fig. 10(a)–(c). Since the Shewhart plots for current, voltage and power shown in Fig. 9(a)–(c) are based on normal operating data, we expect that almost all the data will lie within the lower and upper control limits. Similarly, the data points in the EWMA charts are also within the 95% confidence limits (see Fig. 10(a)–(c)). It can be concluded that the ODM model describes the data well when no faults are present.

5.1.2. Case study of open-circuit PV strings

In this case study, the performance of the two monitoring charts when there is an open-circuit fault is investigated. To do so, an open-circuit fault in a PV array is introduced by disconnecting the second string from the monitored PV system (see fault #1 in Fig. 11) between sample times 300–500.

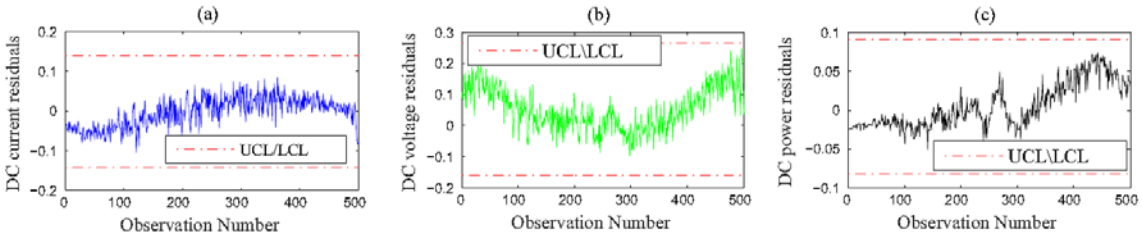

Fig. 9. Monitoring results of a Shewhart chart for DC current (a), DC voltage (b) and DC power (c) under normal operating conditions.

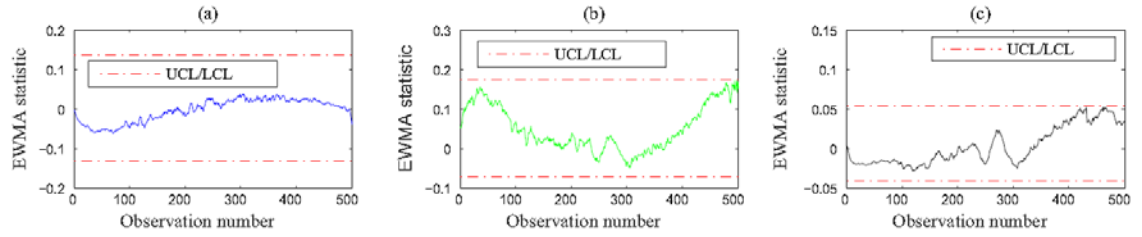

Fig. 10. Monitoring results of EWMA chart for DC current (a), DC voltage (b) and DC power (c) under normal operating conditions.

To monitor the PV system, the residuals (i.e.,eI ; eV and eP) are first computed. Then both monitoring charts, Shewhart and EWMA, are used for fault detection. The Shewhart and EWMA charts based on the MPP residuals of current, voltage and power are presented in Figs. 12 and 13, respectively. The shaded area is the region where the fault is introduced. The plots in Figs. 12(c) and 13(c) indicate that before the occurrence of the fault, both charts are within the lower and upper control limits. The PV system is thus working normally.

For this case, the two charts can both give fault signals because the introduced fault is quite large. Figs. 12(c) and 13(c), show that the Shewhart and EWMA charts based on the output power residuals, eP, decrease significantly and exceed the lower control limits, indicating that there is a significant power loss.

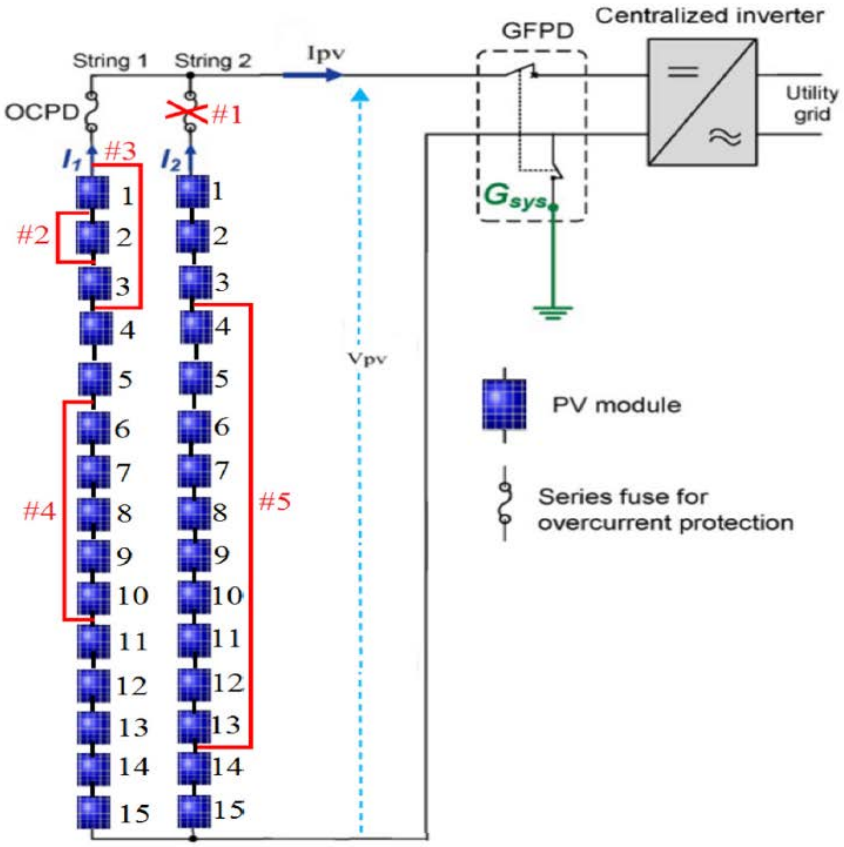

Fig. 11. Open-circuit and short-circuit faults.

Since one of the two strings of a PV array is disconnected at the fault, a large amount of power (nearly 50% of the rated power) is lost. After detecting the presence of a fault, the monitoring results related to the output DC current and voltage are analyzed to identify the type of fault. Both Figs. 12(b) and 13(b) are within the lower and upper control limits before and after the fault, which means that the DC voltage is almost the same after the occurrence of this open-circuit fault. The two monitoring charts based on the current residuals are given in Figs. 12(a) and 13(a). These charts show that both charts exceed the lower control limits, indicating the presence of a faulty string (open-circuit fault). Indeed, the current of the faulty string drops to zero when the string is disconnected from the PV array. As a result, the residuals, which indicate the difference between the simulated and measured DC current, decrease immediately after the occurrence of the open-circuit fault. From this case study, it can be seen that the open-circuit fault in a PV array increases the power loss, reduces the array current and results in almost the same array voltage as the normal PV array voltage. These results indicate the efficiency of both fault detection strategies in detecting and diagnosing open-circuit faults in a PV system.

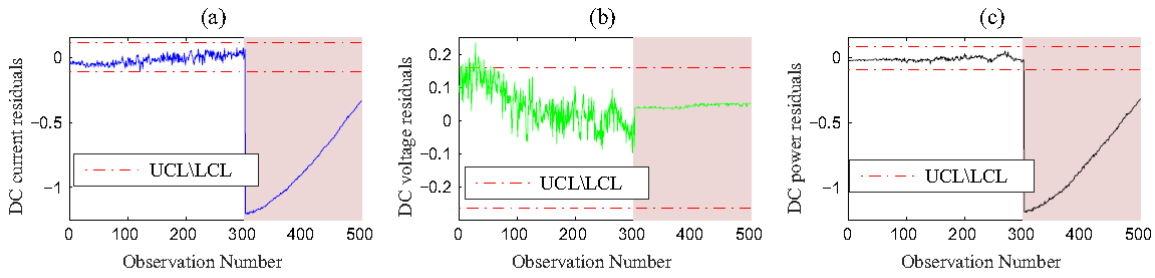

Fig. 12. Monitoring results of a Shewhart chart for DC current (a), DC voltage (b) and DC power (c) in the presence of an open-circuit fault.

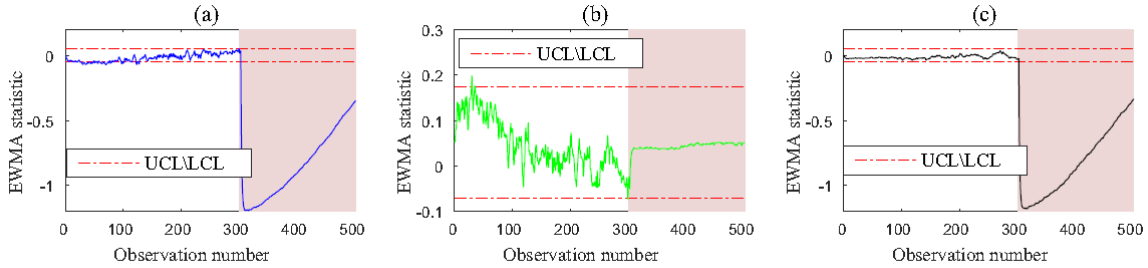

Fig. 13. Monitoring results of an EWMA chart for DC current (a), DC voltage (b) and DC power (c) in the presence of an open-circuit fault.

5.1.3. Case study of a short circuit in a string of PV modules

In this case study, the detection of short-circuited PV modules in the monitored PV system is investigated. Four examples are given in this case study (see Fig. 11, faults #2–#5).

(1) One short-circuited PV module: In the first example, the second module of the first string is bypassed from observation number 300 until the end of the testing data (see Fig. 11, fault #2). The output DC current, voltage and power were monitored using Shewhart and EWMA charts. The two monitoring charts are shown in Fig. 14(a)–(c) and Fig. 15(a)–(c). Fig. 14 shows that the Shewhart chart cannot detect this fault. The Shewhart chart is insensitive to this fault because it is designed to detect relatively moderate and large faults, while the fault in this case is quite small. This is mainly due to the fact that the Shewhart chart uses only observed data at a particular instant to make a decision about the process performance and it ignores past data. On the other hand, the plot in Fig. 15(c) clearly shows the capability of the EWMA monitoring chart in detecting this small fault. From the plots in Fig. 15(a) and (b), it can be seen that the DC current residuals are within the control limits, while the DC voltage residuals exceeds the lower control limit. Thus, we can conclude that the detected fault is related to a faulty module in the string. This case study clearly shows the superiority of the EWMA over the Shewhart chart in detecting small faults.

(2) Three short-circuited PV modules: In the second example, three modules have been short circuited in the first string (see Fig. 11, fault #3). The monitoring results of the Shewhart and EWMA charts are shown in Figs. 16 and 17, respectively. The performance of the Shewhart chart when it is applied to the output power residuals is presented in Fig. 16(c), which shows that the Shewhart statistic clearly violates the lower control limit. The Shewhart chart detects this fault (i.e., a power loss) but it misses some data. On the other hand, the plot in Fig. 17(c) clearly shows the capability of the EWMA monitoring chart in correctly detecting this moderate fault without missed data. This short-circuit fault degrades the performance of the monitored systems and leads to a significant power loss (i.e., approximatively 15% power loss).

After detecting a fault based on the output DC power, the two monitoring charts based on residuals of output DC current and voltage, which are shown in Figs. 16(a) and (b) and 17(a) and

(b), can provide more information about the type of fault. Both Figs. 16(b) and 17(b) show fault signals because the decrease in output DC voltage in this case is quite large. The output DC current from the array does not change by much. Because the output DC voltage decreases compared to the output DC voltage of the normal array and the output DC current does not change by much, we then conclude that this fault is a short circuit in the PV array.

(3) Five short-circuited PV modules: In the third example, five modules in first string are disconnected (Fig. 11, fault #4). This fault leads to a power loss of 30% compared to the healthy PV array. Both monitoring charts can detect this quite large fault as shown in Figs. 18(c) and 19(c). Similar to the cases above, to identify this fault, we look at the monitoring results related to the array voltage and current (see Figs. 18(a) and (b) and 19(a) and (b)). In fact, it is a fault that corresponds to a short-circuited PV module, since both charts based on voltage are below the control limits (see Figs. 18(b) and 19(b)), and the current does not change by much (see Figs. 18 (a) and 19(a)). This demonstrates the effectiveness of the proposed strategy in detecting and identifying faults related to shortcircuited modules.

(4) Ten short-circuited PV modules: In the fourth example, ten modules in the second string of the monitored PV array were short circuited (see Fig. 11, fault #5). Indeed, the fault resulted in large voltage drops and significant power loss (i.e. nearly 63%). Both monitoring charts can clearly detect and identify this quite large fault (see Figs. 20(a)–(c) and 21(a)–(c)).

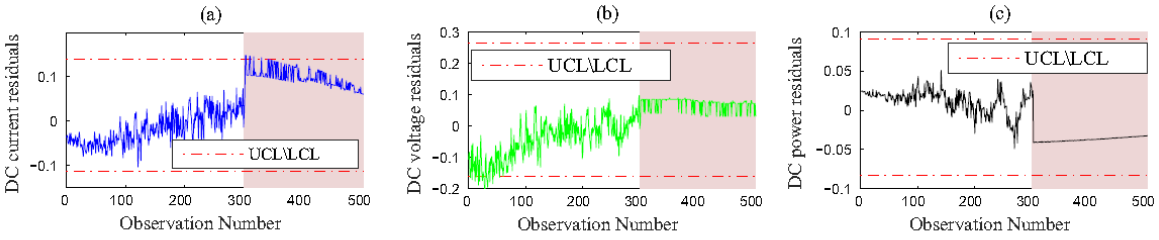

Fig. 14. Monitoring results of a Shewhart chart for DC current (a), DC voltage (b) and DC power (c) in the presence of one short-circuited module.

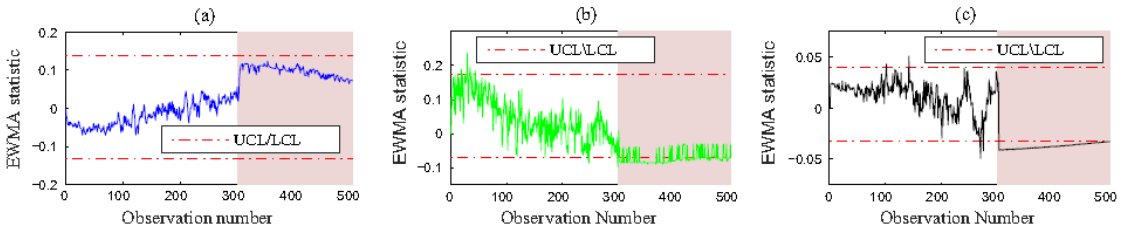

Fig. 15. Monitoring results of an EWMA chart for DC current (a), DC voltage (b) and DC power (c) in the presence of one short-circuited module.

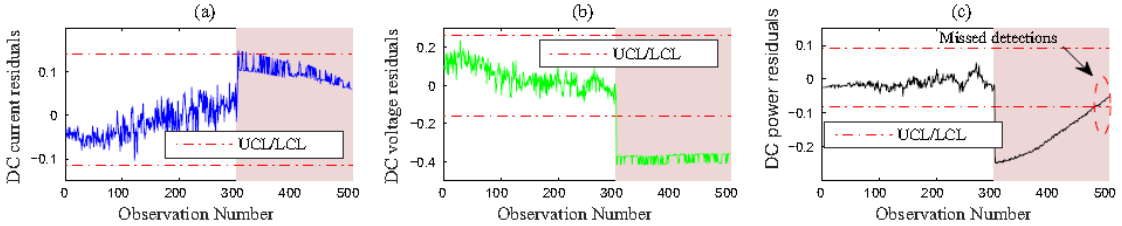

Fig. 16. Monitoring results of a Shewhart chart for DC current (a), DC voltage (b) and DC power (c) in the presence of three short-circuited modules in a PV array.

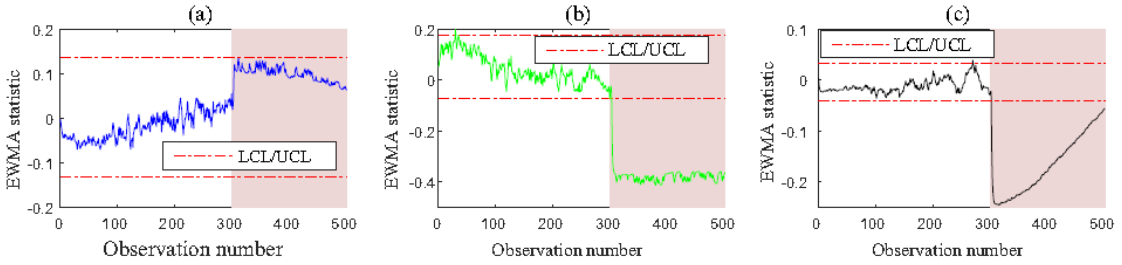

Fig. 17. Monitoring results of an EWMA chart for DC current (a), DC voltage (b) and DC power (c) in the presence of three short-circuited modules in a PV array.

517

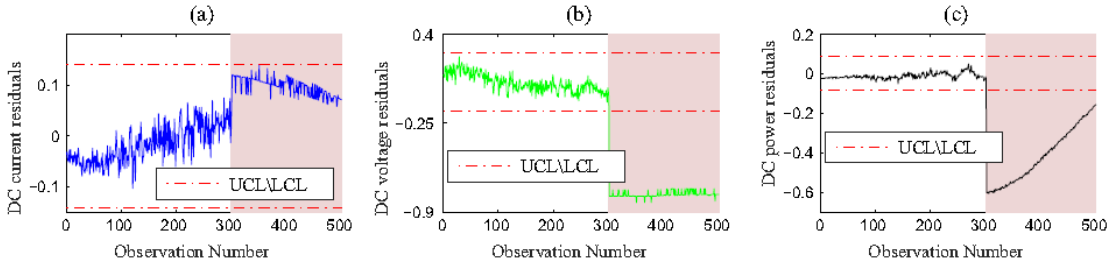

Fig. 18. Monitoring results of a Shewhart chart for DC current (a), DC voltage (b) and DC power (c) in the presence of five short-circuited modules in a PV array.

518

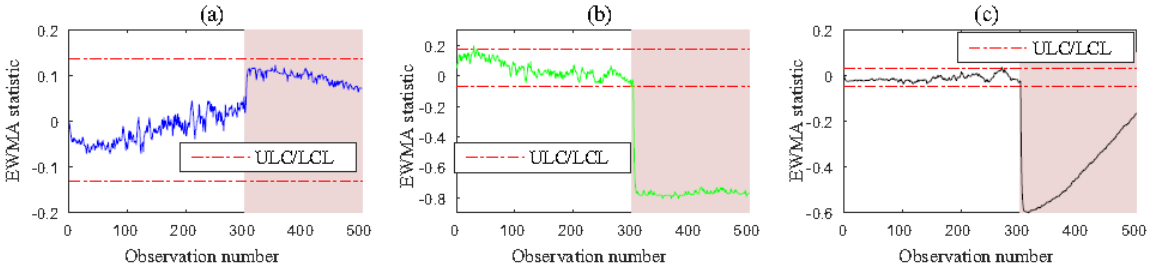

Fig. 19. Monitoring results of an EWMA chart for DC current (a), DC voltage (b) and DC power (c) in the presence of five short-circuited modules in a PV array.

519
520
521

5.1.4. Case study of shading fault

The aim of this case study was to assess the potential of the proposed ODM-based EWMA method to detect and identify partial shading faults in a PV system.

(1) Temporarily shading of four PV modules: In this example, the first four modules of the PV system were temporarily fully shaded (see Fig. 22, fault #6), between samples 150 and 250. Figs. 23 and 24 show that both charts can detect and identify this fault. This type of fault may cause decreases in current and voltage and significant power loss.

(2) Fully shading of one PV module: In this example, the module number 14 of the first string of the PV system were temporarily exposed to fully shading (see Fig. 22, fault #7), between samples 150 and 250. The shewhart chart fails to detect this fault, as shown in Fig. 25(a)–(c). Fig. 26(c) shows that the EWMA chart is able to detect the fault, but it cannot identify its type (see Fig. 26(b) and (c)).

5.1.5. Case study of multiple faults

To assess the capacity of the proposed method to detect multiple faults, five modules in the PV system were exposed to a partial shading (Fig. 22, fault #6), between samples 150 and 250, and then five modules in one string were short-circuited (Fig. 22, fault #8).

Monitoring results of the Shewhart and EWMA charts are illustrated in Figs. 27 and 28, respectively. In this case, both charts can accurately detect and identify these multiple faults.

In summary, our ODM-EWMA fault detection scheme provides satisfactory results in detecting and identifying short-circuit faults, open-circuit faults in PV strings and partial shading. In addition, to detect small changes (e.g., one short-circuited module in a string), the EWMA chart is more effective.

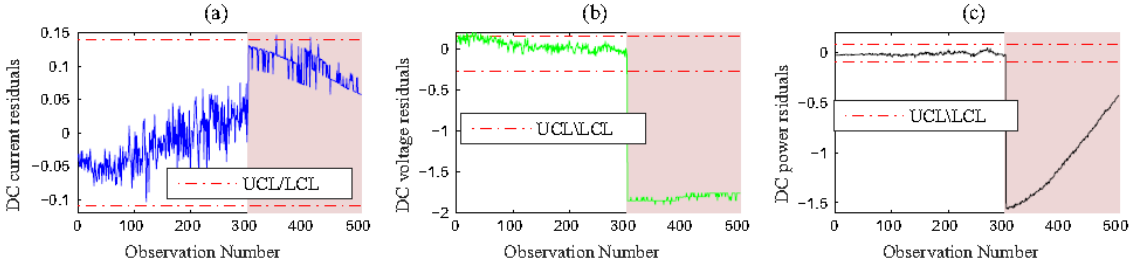

Fig. 20. Monitoring results of a Shewhart chart for DC current (a), DC voltage (b) and DC power (c) in the presence of ten short-circuited modules in a PV array.

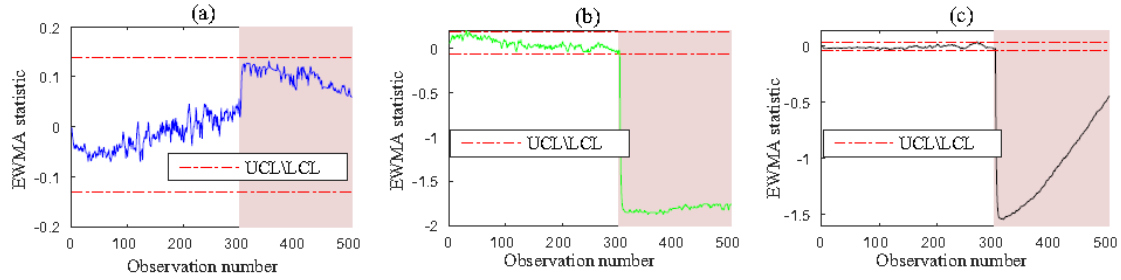

Fig. 21. Monitoring results of an EWMA chart for DC current (a), DC voltage (b) and DC power (c) in the presence of ten short-circuited modules in a PV array.

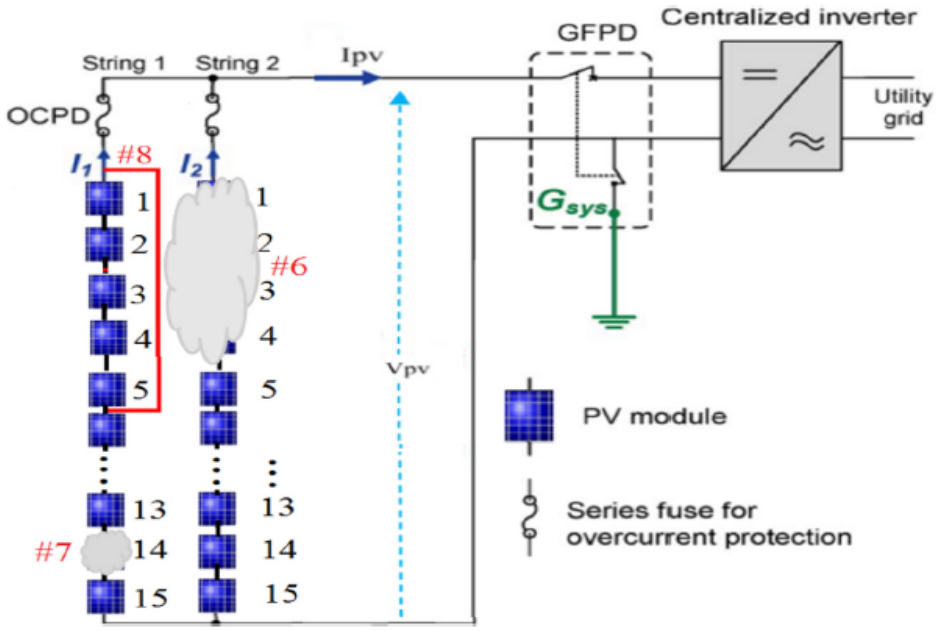

Fig. 22. Typical faults in a PV array: temporarily shading and faulty modules.

546

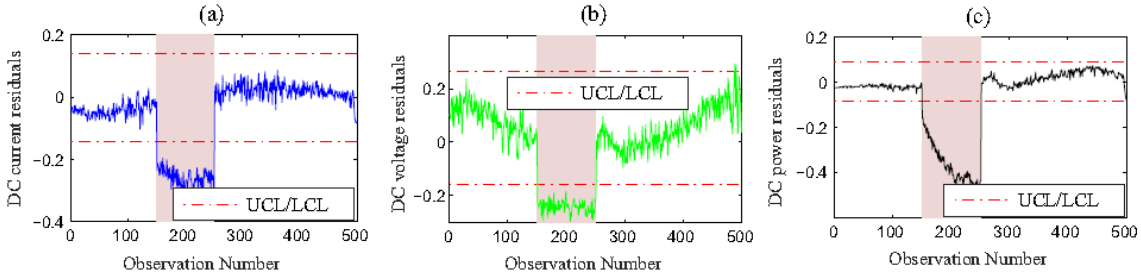

Fig. 23. Monitoring results of Shewhart chart for DC current (a), DC voltage (b) and DC power (c) in the presence of 4 PV modules temporarily shaded in the PV system

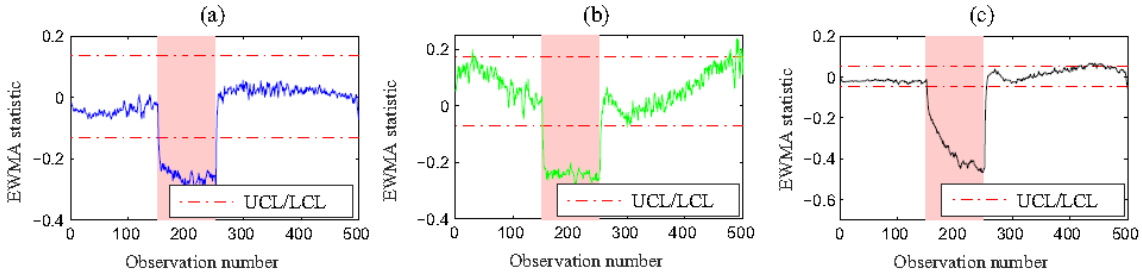

Fig. 24. Monitoring results of EWMA chart for DC current (a), DC voltage (b) and DC power (c) in the presence of 4 PV modules temporarily shaded in the PV system.

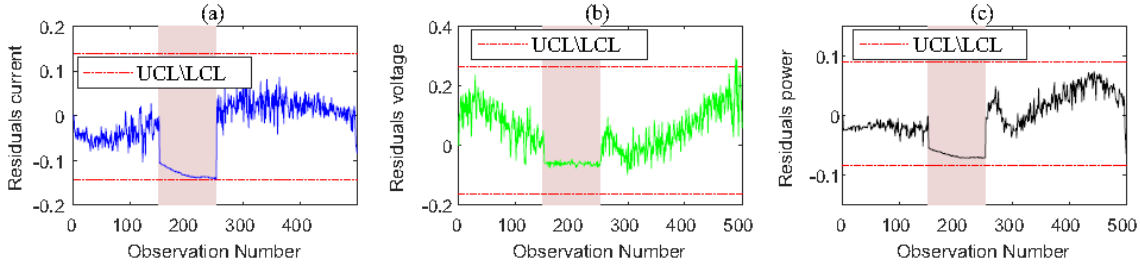

Fig. 25. Monitoring results of Shewhart chart for DC current (a), DC voltage (b) and DC power (c) in the presence of 4 PV modules fully shaded in the PV system.

547

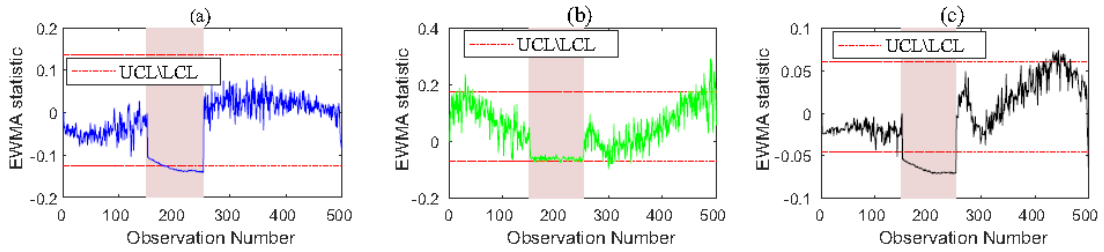

Fig. 26. Monitoring results of EWMA chart for DC current (a), DC voltage (b) and DC power (c) in the presence of one PV module fully shaded in the PV system.

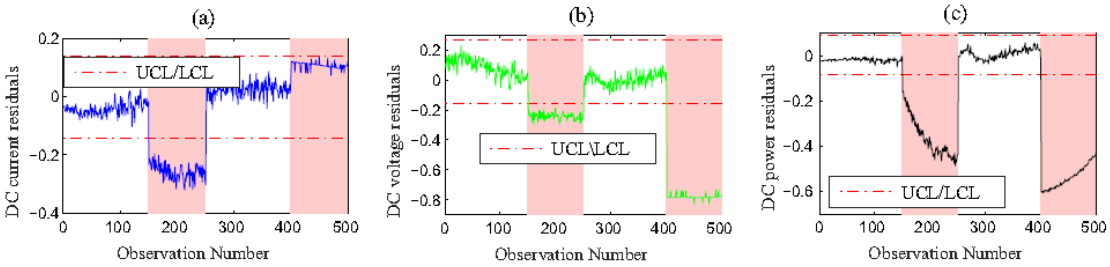

Fig. 27. Monitoring results of a Shewhart chart for DC current (a), DC voltage (b) and DC power (c) in the presence of 4 PV modules that are partially shaded and five short-circuited modules in the PV system.

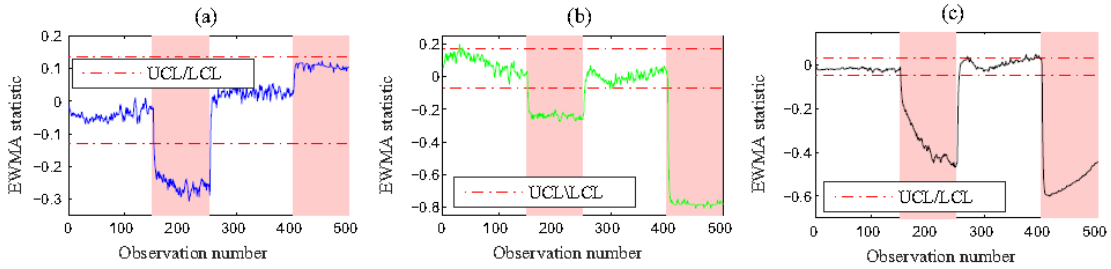

Fig. 28. Monitoring results of an EWMA chart for DC current (a), DC voltage (b) and DC power (c) in the presence of4 PV modules that are partially shaded and five short-circuited modules in the PV system.

6. Conclusion

Solar-energy-based photovoltaic (PV) systems are increasingly gaining worldwide attention due to the high electricity consumption in combination with the desired environmental friendly solutions for power production development. Indeed, PV systems are continuously exposed to many factors that significantly degrade their performances and efficiency. Faults such as short-circuit, open circuit and shading in PV systems can reduce solar energy productivity, leading to economic losses. This paper reports the development of a statistical fault detection approach for monitoring the performances of PV systems by detecting faults on the DC side and diagnosing the type of detected fault. This approach uses a simulation model based on the extracted ODM model parameters to predict the maximum current, voltage and power generated from the PV system. Residuals, which are the difference between measured and predicted variables, are used as input for the EWMA chart. Then, the EWMA based on residuals of output DC power is used to identify, in real time, the presence of faults in the monitored system. Voltage and current residuals are used to differentiate between open-circuit faults, short-circuit faults and partial shading in a PV system. Using practical data from a grid connected PV system at CDER in Algeria, the effectiveness of ODM-EWMA to detect and identify faults in an actual PV system has been demonstrated.

Despite the promising results for fault detection and diagnosis obtained using the ODM-EWMA approach, the work carried out in this paper raises a number of questions and provides some directions for future works. In particular, the following points merit consideration from researchers.

Beside fault detection and diagnosis capability, the EWMA chart is able to capture fault severity (amplitude). The larger the fault is, the greater the amplitude of the EWMA statistic compared to its amplitude under healthy conditions. Therefore, this approach can be extended to determine the number of faulty PV strings and/or PV modules.

Herein, the diagnosis of the fault is done on the basis of only the MPP coordinates of current and voltage to identify the type of fault. In fact, the shading of one PV module or small portion of PV module does not necessarily affect simultaneously current and voltage MPP coordinates. Hence the proposed diagnosis method cannot correctly discriminate this fault. To bypass this shortcoming, we plan to include more input data such as open circuit voltage (Voc), short circuit current (Isc) and fill factor (FF) since they are affected significantly by shading fault.

The presence of noisy and correlated data makes the fault detection more difficult as the presence of noise degrades fault detection quality and most methods are developed for independent observations. In fact, wavelet-based multiscale representation of data has been shown to provide effective noise-feature separation in the data and to approximately decorrelate the auto-correlated data. As future work, the aim is to develop multiscale EWMA fault detection methods that can provide enhanced performances of this technique, especially when data observed from PV system are noisy and highly autocorrelated.

Acknowledgement

We would like to thank the reviewers of this article for their insightful comments, which helped us to greatly improve its quality.

This publication is based upon work supported by King Abdullah University of Science and Technology (KAUST), Office of Sponsored Research (OSR) under Award No: OSR-2015-CRG4-2582. The authors (Elyes Garoudja and Kamel Kara) thank the SET Laboratory, Department of Electronics, Faculty of Technology, University of Blida 1, Algeria, for continuous support during the study.

References

Abou, S., Chouder, A., Kara, K., Silvestre, S., 2015. Artificial bee colony based algorithm for maximum power point tracking (MPPT) for PV systems operating under partial shaded conditions. Appl. Soft Comput. 32, 38–48.

Alam, M., Khan, F., Johnson, J., Flicker, J., 2015. A comprehensive review of catastrophic faults in PV arrays: types, detection, and mitigation techniques. IEEE J. Photovoltaics 5 (3), 982–997.

Arab, A., Cherfa, F., Chouder, A., Chenlo, F., 2005. Grid-connected photovoltaic system at CDER-algeria. In: 20th European Photovoltaic Solar Energy Conference and Exhibition, Barcelone, pp. 6–10.

Brooks, B., 2011. The bakersfield fire: a lesson in ground-fault protection. SolarPro 4 (2).

Chao, K., Ho, S., Wang, M., 2008. Modeling and fault diagnosis of a photovoltaic

615 system. Electr. Power Syst. Res. 78 (1), 97–105.
616 Chine, W., Mellit, A., Lughi, V., Malek, A., Sulligoi, G., Pavan, A., 2016. A novel fault
617 diagnosis technique for photovoltaic systems based on artificial neural
618 networks. Renew. Energy 90, 501–512.
619 Chouder, A., Silvestre, S., 2009. Analysis model of mismatch power losses in PV
620 systems. J. Sol. Energy Eng. 131 (2), 024504.
621 Chouder, A., Silvestre, S., 2010. Automatic supervision and fault detection of PV
622 systems based on power losses analysis. Energy Convers. Manage. 51 (10),
623 1929–1937.
624 Duffie, J., Beckman, W., 2013. Solar Engineering of Thermal Processes, vol. 3. Wiley,
625 New York.
626 Garoudja, E., Kara, K., Chouder, A., Silvestre, S., 2015. Parameters extraction of
627 photovoltaic module for long-term prediction using artificial bee colony
628 optimization. In: 3rd International Conference on Control, Engineering &
629 Information Technology (CEIT). IEEE, pp. 1–6.
630 Hachana, O., Tina, G., Hemsas, K., 2016. PV array fault diagnostic technique for BIPV
631 systems. Energy Build. 126, 263–274.
632 Hare, J., Shi, X., Gupta, S., Bazzi, A., 2016. Fault diagnostics in smart micro-grids: a
633 survey. Renew. Sustain. Energy Rev. 60, 1114–1124.
634 Hariharan, R., Chakkarapani, M., Ilango, G., Nagamani, C., 2016. A method to detect
635 photovoltaic array faults and partial shading in PV systems. IEEE J. Photovoltaics
636 6 (5), 1278–1285.
637 Harrou, F., Fillatre, L., Nikiforov, I., 2014. Anomaly detection/detectability for a
638 linear model with a bounded nuisance parameter. Ann. Rev. Contr. 38 (1), 32–
639 44.
640 Harrou, F., Nounou, M., 2014. Monitoring linear antenna arrays using an
641 exponentially weighted moving average-based fault detection scheme. Syst.
642 Sci. Contr. Eng.: Open Access J. 2 (1), 433–443.
643 Harrou, F., Nounou, M., Nounou, H., Madakyaru, M., 2015. PLS-based EWMA fault
644 detection strategy for process monitoring. J. Loss Prev. Process Ind. 36, 108–119.
645 Hu, Y., Cao, W., Wu, J., Ji, B., Holliday, D., 2014. Thermography-based virtual MPPT
646 scheme for improving PV energy efficiency under partial shading conditions.
647 IEEE Trans. Power Electron. 29 (11), 5667–5672.
648 Hunter, J.S., 1986. The exponentially weighted moving average. J. Qual. Technol. 18
649 (4), 203–210.
650 Johansson, T., 1993. Renewable Energy: Sources for Fuels and Electricity. Island
651 Press.
652 Johnson, J., Kuszmaul, S., Bower, W., Schoenwald, D., 2011. Using PV module and
653 line frequency response data to create robust arc fault detectors. In:
654 Proceedings of the 26th European Photovoltaic Solar Energy Conference and
655 Exhibition, pp. 05–09.
656 Kadri, F., Harrou, F., Chaabane, S., Sun, Y., Tahon, C., 2016. Seasonal ARMA-based SPC
657 charts for anomaly detection: application to emergency department systems.
658 Neurocomputing 173, 2102–2114.
659 Kang, B., Kim, S., Bae, S., Park, J., 2012. Diagnosis of output power lowering in a PV
660 array by using the Kalman-filter algorithm. IEEE Trans. Energy Convers. 27 (4),
661 885–894.
662 Lucas, J., Saccucci, M., 1990. Exponentially weighted moving average control

663 schemes: properties and enhancements. Technometrics 32 (1), 1–12.
664 McEvoy, A., Castaner, L., Markvart, T., 2012. Solar Cells: Materials, Manufacture and
665 Operation. Academic Press.
666 Mekki, H., Mellit, A., Salhi, H.H., 2016. Artificial neural network-based modelling
667 and fault detection of partial shaded photovoltaic modules. Simul. Model. Pract.
668 Theory 67, 1–13.
669 Montgomery, D., 2007. Introduction to Statistical Quality Control. John Wiley &
670 Sons.
671 Montgomery, D.C., 2005. Introduction to Statistical Quality Control. John Wiley&
672 Sons, New York.
673 Munoz, M., Alonso-Garcia, M., Vela, N., Chenlo, F., 2011. Early degradation of silicon
674 PV modules and guaranty conditions. Sol. Energy 85 (9), 2264–2274.
675 Panwar, N., Kaushik, S., Kothari, S., 2011. Role of renewable energy sources in
676 environmental protection: a review. Renew. Sustain. Energy Rev. 15 (3), 1513–
677 1524.
678 Pavan, A., Mellit, A., Pieri, D., Kalogirou, S., 2013. A comparison between BNN and
679 regression polynomial methods for the evaluation of the effect of soiling in large
680 scale photovoltaic plants. Appl. Energy 108, 392–401.
681 Platon, R., Martel, J., Woodruff, N., Chau, T., 2015. Online fault detection in PV
682 systems. IEEE Trans. Sustain. Energy 6 (4), 1200–1207.
683 Reynolds, M., Stoumbos, Z., 2005. Should exponentially weighted moving average
684 and cumulative sum charts be used with Shewhart limits? Technometrics 47
685 (4), 409–424.
686 Shrikhande, S., Varde, P., Datta, D., 2016. Prognostics and health management:
687 methodologies & soft computing techniques. In: Current Trends in Reliability,
688 Availability, Maintainability and Safety. Springer, pp. 213–227.
689 Silvestre, S., daSilva, M., Chouder, A., Guasch, D., Karatepe, E., 2014. New procedure
690 for fault detection in grid connected PV systems based on the evaluation of
691 current and voltage indicators. Energy Convers. Manage. 86, 241–249.
692 Silvestre, S., Kichou, S., Chouder, A., Nofuentes, G., Karatepe, E., 2015. Analysis of
693 current and voltage indicators in grid connected PV (photovoltaic) systems
694 working in faulty and partial shading conditions. Energy 86, 42–50.
695 Suganthi, L., Iniyan, S., Samuel, A., 2015. Applications of fuzzy logic in renewable
696 energy systems – a review. Renew. Sustain. Energy Rev. 48, 585–607.
697 Tadj, M., Benmouiza, K., Cheknane, A., Silvestre, S., 2014. Improving the
698 performance of PV systems by faults detection using GISTEL approach. Energy
699 Convers. Manage. 80, 298–304.
700 Vergura, S., Acciani, G., Amoruso, V., Patrono, G., Vacca, F., 2009. Descriptive and
701 inferential statistics for supervising and monitoring the operation of PV plants.
702 IEEE Trans. Ind. Electron. 56 (11), 4456–4464.
703 Yahyaoui, I., Segatto, M., 2017. A practical technique for on-line monitoring of a
704 photovoltaic plant connected to a single-phase grid. Energy Convers. Manage.
705 132, 198–206.
706 Zerrouki, N., Harrou, F., Sun, Y., Houacine, A., 2016. Accelerometer and camerabased
707 strategy for improved human fall detection. J. Med. Syst. 40 (12), 284.
708 Zhao, Y., Ball, R., Mosesian, J., dePalma, J., Lehman, B., 2015. Graph-based semisupervised
709 learning for fault detection and classification in solar photovoltaic
710 arrays. IEEE Trans. Power Electron. 30 (5), 2848–2858.

711 Zhao, Y., dePalma, J., Mosesian, J., Lyons, R., Lehman, B., 2013. Line–line fault
712 analysis and protection challenges in solar photovoltaic arrays. IEEE Trans. Ind.
713 Electron. 60 (9), 3784–3795.